Synthesis of α^{″}-Fe_{16}N_{2} Compound Anisotropic Magnet by the Strained-Wire Method

Yanfeng Jiang, Vivekanand Dabade, Lawrence F. Allard, Edgar Lara-Curzio, Richard James, and Jian-Ping Wang

Phys. Rev. Applied **6**, 024013 — Published 18 August 2016

DOI: 10.1103/PhysRevApplied.6.024013

Synthesis of α˝-$Fe_{16}N_2$ Compound Anisotropic Magnet by a Strained Wire Method

Yanfeng Jiang[1], Vivekanand Dabade[2], Lawrence F.Allard[3], Edgar Lara-Curzio[3], Richard James[2], Jian-Ping Wang [1,*]

[1] Department of Electrical and Computer Engineering, University of Minnesota, Minneapolis, Minnesota 55455, USA
[2]Department of Aerospace Engineering and Mechanics, University of Minnesota, Minneapolis, Minnesota 55455, USA
[3] Materials Science and Technology Division, Oak Ridge National Laboratory, Tennessee 37831, USA
*Corresponding author (E-mail address: jpwang@umn.edu)

Abstract α"-$Fe_{16}N_2$ is considered as one of the most promising candidates for future rare-earth-free magnets, showing the highest saturation magnetization reported so far. We propose and demonstrate a novel "strained wire method" to synthesize α˝-$Fe_{16}N_2$ compound anisotropic magnets with enhanced hard magnetic property, with a direct experimental observation of the inter-coupling between tensile strain and the martensitic phase transition. The principal is helpful for the generation of other martensitic phase. In this paper, the method is demonstrated on an α"-$Fe_{16}N_2$ compound permanent magnet preparation by starting from pure bulk iron, with urea as the nitrogen provider. A uniaxial tensile stress is applied on the wire-shaped sample during the post-annealing stage, producing a promising permanent magnet with hard magnet property which lacks any rare-earth elements. The sample synthesized in the lab exhibits coercivity of 1220 Oe and an energy product of up to 9 MGOe. The mechanism of the strained wire method is analyzed based on Scanning Transmission Electron Microscopy (STEM) characterizations of samples with different strains. This is the first time a strain-induced recrystallization of α"-$Fe_{16}N_2$ samples at low annealing temperature (150 ^{o}C) has been observed. We demonstrate that this strained wire method can be used on α"-$Fe_{16}N_2$ samples to increase the α"-$Fe_{16}N_2$ phase-volume ratio and to fine tune its microstructure at low temperature. Some further characterization results are also included in this paper. The physics of the influence of tensile stress on the martensitic phase transition is discussed.

PACS: 75.50.Ww

I. INTRODUCTION

Advanced permanent magnet materials provide high efficiency and reliability, low cost, and low maintenance solutions for renewable energy technologies. Unfortunately, currently used rare earth permanent magnets have supply constraints and high prices. A new magnet with more abundant and less strategically important elements is required to replace rare earth magnets. α˝-$Fe_{16}N_2$ is considered a potential candidate for rare-earth-free magnets with a high energy product because of its giant saturation magnetization and large magnetocrystalline anisotropy[1,2]. Although this material has such promising magnetic property and is obviously beneficial for our future environment, there are still no reports about bulk FeN permanent magnets because the nitrifying of iron, the body central tetragonal

phase induction, grain structure and domain alignment are major obstacles. An effective synthesis route is needed to prepare this unique magnet.

α″-$Fe_{16}N_2$ phase was first discovered by Jack[3], but its magnetic properties remained unexplored until 1972 when Kim and Takahashi[4] reported its high magnetization in thin films obtained by evaporating iron onto a glass substrate in low-pressure nitrogen. This discovery has inspired many groups all over the world to explore the material by using different synthesis techniques[2,5-16].

Encouraged by the promising magnetic properties demonstrated by thin films, researchers have been interested in preparing bulk samples with a larger volume fraction of $Fe_{16}N_2$ phase while exhibiting the same promising magnetic properties[8,11,14]. These experiments have essentially followed Jack's early approach[3] via γ and α′ phases. However, none of the above bulk synthesis methods showed the possibility of producing permanent magnets because of the relatively low coercivity values obtained. Current synthesis methods for $Fe_{16}N_2$ magnets adopts iron powder or thin foil as a precursor, which can be nitridized easily, followed by sintering or shocking to form a bulk shape[17-21]. For example, Ogi *et al.* used a gas-phase method to synthesize Al_2O_3 coated α″-$Fe_{16}N_2$ spherical nanoparticles with Ms to be 162 emu/g and coercivity up to 3070 Oe[17]. We have previously used a ball milling method to prepare α″-$Fe_{16}N_2$ particles and then compacted them into a disc magnet with the shock-compaction method[18]. Very recently, a free standing FeN foil (500 nm in thickness) with energy product up to 20 MGOe has been reported by our group recently, in which ion implantation is used for nitrogen atom introduction[19].

Until now, the reported coercive force of $Fe_{16}N_2$ materials in bulk format is still too small to be used practically. To improve its coercivity, its microstructure would be tuned into suitable grain size with an obvious boundary. However, the grain size and grain boundary of α″-$Fe_{16}N_2$ magnet is hardly to be tuned by traditional approaches. The main reason is that α″-$Fe_{16}N_2$ is martensite phase and can only be stable under 214 ^{o}C. However, the minimum temperature to adjust the microstructure of α″-$Fe_{16}N_2$ is 350 ^{o}C[22], as shown in FIG.S1 in supplementary materials23 . Therefore, the normal annealing approach is not suitable for α″-$Fe_{16}N_2$ magnet. To prevent the martensitic phase decomposition, a low temperature approach to tune the microstructure to enhance the coercive force of α″-$Fe_{16}N_2$ magnet is highly required.

To assist the martensitic phase transformation from bcc to bct during a low temperature annealing process, extra energy is needed to compensate for the shortage of the thermal energy. The methods include applying external stress and magnetic field. We have previously shown the influence of magnetic field on α"-$Fe_{16}N_2$ martensitic phase transition[24], in which phase transformation from α' to α" increasing up to 78%. The working principle of the improved phase transition assisted by external force, either magnetic field or external stress, is shown in FIG.1. The crystal structures of bcc and bct are also shown in the figure. The main difference of crystalline structure between bcc and bct is the lattice constant of c-axis. The bct structure has an elongated c-axis compared to that of bcc phase. During nitriding process, nitrogen atoms are introduced in the octahedral interstices in a random manner with equal possibility on every orientation. With the assistance of stress along c-axis, as shown in FIG.1, (001) axis would be turned into the most preferred position for nitrogen atoms because the elongated axis corresponds to

the lowest energy state. In this way, suitable stress along c-axis should be useful for bct phase transformation. This is the starting point to propose a "strained wire method" as discussed in following.

In this paper, an external stress is adopted for the material preparation. The method is termed the "strained wire method" because an external force is applied during the post-annealing stage to assist the martensitic phase transformation and the microstructure reconstruction. We experimentally demonstrated that the strained wire method could be used to tune the magnetic properties at a low annealing temperature (<180 ^{o} C). Both the remanence and coercivity of the samples are improved, showing an anisotropic permanent magnetic property.

II. EXPERIMENTAL RESULTS

The α''-$Fe_{16}N_2$ bulk permanent magnet was prepared from commercially available bulk iron of high purity (99.99%). Here, urea was used as a nitrogen provider in the cold crucible system (Crystalox Bridgman Stockbarger System). First, the bulk iron was melted in the cold crucible system with a prefixed percentage of urea. Urea was chemically decomposed to generate nitrogen atoms. In the second step, the prepared FeN mixture was removed from the cold crucible system and heated to 660 °C for 4 hrs and then quenched with water at room temperature. After that, the quenched sample was flattened and cut into square, column wires, 0.2-0.3 mm^2 and 10 mm long. During the following annealing step, wires were strained using a loading device to apply an external force to the elongate the length of the lattice. Detail information of the whole process description and the schematic of the loading device can be found in supporting material23.

The strained wire method leads to a bulk FeN with promising hard magnet properties. FIG.2 shows the characterization results. The hysteresis loop is shown in FIG. 2(a) and the X-ray diffraction (XRD) pattern in FIG.2(b). Hysteresis loop 'a' shows the magnetic property of the prepared FeN magnet, with coercivity of up to 1220 Oe while the saturation magnetization (M_s) at the 2 T field is 220 emu/g. The energy product at room temperature is tested to be 9 MGOe. Hysteresis loop 'b' in FIG.2(a) corresponds to that of pure iron and is used as a reference. It is seen clearly that both the coercivity and saturation magnetization of the prepared FeN sample are improved dramatically compared to that of pure iron. The XRD pattern of the FeN sample, as shown in FIG. 2(b), demonstrates the existence of an $Fe_{16}N_2$ phase in the sample. The prepared sample is a mixture of $Fe_{16}N_2$, Fe_8N, Fe_4N and Fe phases. The microstructure of the sample is shown in FIG.2(c), from a high angle annular dark-field (HAADF) image of a focused ion-beam-milled cross section (Hitachi NB-5000 FIB mill). The crystallography of the Fe-N sample is determined in part by direct electron micro-diffraction experiments in the Hitachi HF-3300 cold field emission TEM, as shown in FIG.2(c). FIG.2(d) shows the actual picture of the prepared bulk FeN magnet.

FIG. 3 shows XRD patterns at the following stages, a) pure iron, b) after cold crucible melting, c) after quenching and d) after post-annealing, respectively. The measurement is characterized using a Siemens D5005 X-ray diffractometer (XRD) with a Cu Kα radiation source.

Compared with the pure iron sample, the FeN sample's crystalline intensity after cold-crucible melting is enhanced by a unidirectional thermal gradient in the crucible during melting and a quick turn-off effect.

The Fe-N phase diagram[25] shows that pure iron transforms into γ phase at temperatures above 590 °C. N-austenite phase (γ phase) is a face center cubic (fcc) arrangement of Fe atoms with N randomly occupying up to one in ten of the octahedral interstices. When γ is quenched below its martensite temperature, Fe atom arrangement changes from fcc to bcc α-Fe. However, N atoms have insufficient time to move from the interstices and the vacancies created by the fcc-bcc transition remain empty. So, a body center tetragonal (bct) martensite phase (α′ phase) of the same composition with austenite phase is generated, and N atoms occupy one in ten of the holes at the midpoints of the c edges and the centers of the C faces[3]. Both the nitrogen atom position and the nitrogen concentration are key points for the generated phase after quenching. As shown in FIG. 3, three phases appear after quenching, including α′-Fe_8N, γ′-Fe_4N and γ-Fe, depending on the local nitrogen concentration.

To assist the phase transformation from α′-Fe_8N to α"-$Fe_{16}N_2$ and also induce an anisotropic behavior of the FeN sample, we propose the "strained wire method" during the post-annealing stage. Detailed information and analysis of this method will be introduced in next section.

Further evidence for the presence of the ordered α"-$Fe_{16}N_2$ phase is given by the aberration-corrected STEM imaging of the structure, as shown in FIG.4. FIG. 4(a) presents the bright-field STEM image while its diffractogram is shown FIG.4(b), clearly indicating an ordered periodic structure with a strong (202) peak in the image. The diffraction patterns consistent with a <202> zone axis orientation of α"-$Fe_{16}N_2$ phase.

III. STRAINED WIRE METHOD

The basic technical route in this paper follows Jack's approach[3], starting from γ-FeN to α′-Fe_8N and finally to α"-$Fe_{16}N_2$ phase. The principle of our proposed strained wire method is to apply a uniaxial tensile force on the prepared wire-shaped sample during the post-annealing stage.

This unconventional method possesses three unique features to enable the synthesis of $Fe_{16}N_2$ bulk magnet. Firstly, the rate of phase transformation from α′-Fe_8N to α"-$Fe_{16}N_2$ is improved. The applied strain induces an elongated lattice along the wire's length orientation, which becomes nitrogen's most preferred position among all possible octahedral interstices. As a result, more α′-Fe_8N phase will be transformed into α"-$Fe_{16}N_2$ phase.

Secondly, the applied strain may help to further tune the microstructure. The annealing temperature for α"-$Fe_{16}N_2$ preparation must be less than 214 ^{o}C based on its phase diagram[25]. However, the minimum temperature to refine the microstructure of α"-$Fe_{16}N_2$ material is 350 ^{o}C[22]. It is, therefore, challenging to refine the microstructure of α"-$Fe_{16}N_2$ without ruining the phase by any traditional approach. However, mechanical deformation can drive crystalline solids far from their equilibrium state by introducing structural or chemical defects. By applying a uniaxial strain on the sample in the plastic deformation region, its microstructure can be tuned at a relatively low temperature. In this way, its coercivity, a microstructure sensitive parameter, can be enhanced under plastic deformation by the applied strain.

The third unique feature of the proposed strained wire method is to enable the alignment of the magnetic easy axis of $Fe_{16}N_2$ grains along the wire in the long axis direction. Although this is clearly demanded for an anisotropic magnet, it has not been reported in any of previous bulk $Fe_{16}N_2$ experiments.

A stretching fixture is set up to generate uniaxial tensile stress and therefore uniaxial strain on the FeN wire sample. For the prepared FeN material, its mechanical properties, including the stress-strain relationship and hardness, are also included in supporting material23. Young's modulus was measured to be 132±3 GPa and the hardness was measured to be 2.4±0.4 GPa.

By applying different strains on samples at different annealing temperatures, the volume ratio of α"-$Fe_{16}N_2$ is summarized in FIG. 5(a), which is calculated based on an XPS method[26]. The error bars come from the calculation process using different fitting functions and different baseline height to get rid of the XPS pattern's noise. At strain level < 0.15%, higher annealing temperatures produce more α"-$Fe_{16}N_2$ phase, whereas with larger strain, the trend changes. The martensite fraction at 180 °C has a reverse tendency with larger applied strain. Its phase volume is reduced to 15.6% under a 0.4% strain, showing that parts of the phase decompose at this situation. For the 120 °C situation, the phase ratio remains almost the same as at larger strains. The 150 °C annealing temperature shows the most promise because the $Fe_{16}N_2$ volume ratio continues to increase as the strain rises. With up to a 0.4% strain, the α˝-$Fe_{16}N_2$ phase ratio increases from 22.4% to 37%. The following magnetic results are all based on the samples produced with the 150 °C annealing temperature.

Magnetic hysteresis loops were obtained at room temperature with a maximum applied field of up to 2 Tesla using a Princeton Measurements vibrating sample magnetometer. Before each measurement, the instrument was calibrated using a standard Ni sample with known magnetic moment (44.4 memu), provided by NIST. The error bar for the moment measurement is less that 2% since the bulk sample can be weighed precisely.

FIG. 5(b) shows room temperature M-H loops for samples annealed with 0.15% strain (loop 'a') and without strain (loop 'b'). Loop 'c' shows the property of the pure iron sample as baseline, with magnetic property that is in good agreement with an Fe (110) single crystal. The saturation magnetization (Ms) of the pure iron sample is around 1.9 T at room temperature (as shown in loop 'c' in FIG.5(b)). Loop 'b' corresponds to the sample prepared by the cold crucible melting, quenching and annealing without strain. It shows an emerging semi-hard magnetic property with coercivity of 204 Oe. More importantly, its Ms increases 10%, which is obviously beyond the VSM testing error. This should attribute to the $Fe_{16}N_2$ phase. The estimated volume ratio for the $Fe_{16}N_2$ phase in this sample is about 22.4%. Thus, the Ms of the $Fe_{16}N_2$ phase in this sample is calculated as 2.56 T. This giant saturation magnetization is consistent with our proposed theory and recent report on thin film samples[2]. Further enhancement of magnetic property can be achieved by using the strained wire method, as shown by loop 'a' in FIG. 5(b) with 0.15% strain. The coercivity increases up to 340 Oe and the Ms up to 2.16 T. These experimental results demonstrate that a uniaxial strain applied during the annealing process could improve the FeN wire sample's magnetic properties, both coercivity and saturation magnetization.

The increment of Ms should be attributed to the fact that the volume ratio of α˝-$Fe_{16}N_2$ has increased to 29.7% with 0.15% strain induction. This means that more phase is transferred from austenite to martensite with the assistance of the external strain. Here one of the most important reasons that strain can influence the magnetic property is closely related to the unique bct crystalline structure of the α˝-$Fe_{16}N_2$[2].

FIG.6 shows the magnetic properties of samples subjected to 0.2% and 0.4% strain during annealing. As shown in FIG. 6(a) and FIG. 6(c), a big jump of coercivity occurs upon application of 0.2% and 0.4% strain, going up to 1200 Oe and 1220 Oe, respectively. The saturation magnetizations are increased at the same time. FIG. 6(b) and FIG. 6(d) show the calculation results for the energy products. The maximum energy products of the sample which underwent 0.2% strain is 4 MGOe, while the maximum energy product of the sample which underwent 0.4% strain is 9 MGOe, emerging as a promising potential low-cost permanent magnet. The energy product boost should be attributed to the squareness of the hysteresis loop with 0.4% strain, as shown in FIG. 6(c).

The magnetic results on different strains are summarized in FIG.7, showing obvious improvement of coercivity and energy product for samples under 0.2% and 0.4% strain.

The above characterizations clearly show that applying uniaxial strain on FeN wires during post-annealing can help increase the volume ratio of the α”-$Fe_{16}N_2$ phase and enhance its hard magnetic properties.

IV. DISCUSSION

It is useful to investigate the mechanism of the strained-wire method and the influence of strain on martensitic phase transformation. It is expected that the strain leads to grain refinement due to the occurrence of recrystallization during the tensile process and to significant improvements in magnetic properties of the material[26]. The study of the influence of the applied strain on grain recrystallization can provide some useful information about the involved processes.

To further understand the effect of applied strained on the microstructure, scanning electron microscopy (SEM) and transmission electron microscopy (TEM) characterizations are carried out on the samples. SEM characterizations (Type: JSM-6610LV) on the samples with different strains at 150 °C annealing temperature for 40 hrs are investigated, as shown in FIG.8, corresponding to 0, 0.15%, 0.2% and 0.4% strain, respectively. The sample with 0.15% strain shows a thread-like structure appearing along the tensile direction, as shown in FIG.8(b). With the strain increasing to 0.2%(FIG.8(c)), the thread-like structure appears with higher density. For the sample under 0.4% strain (FIG.8(d)), more thread-like structures with additional visible planar defects and small grains emerge.

FIG.9 shows the high-resolution STEM characterizations on the samples as shown in FIG.8. For the sample without strain, as shown in FIG. 9(a), the STEM characterizations have an amorphous contour since the annealing temperature is too low for crystallization. For the sample under 0.15% strain,

defects begin to appear. The defects appear more and more obviously as the strain increases, as shown in FIG. 9(c) and (d). For the sample with 0.4% strain, the defects have formed a sealed boundary and generated a whole grain. Obvious nano-crystallization is observed in the sample under 0.4% strain. Such tensile-stress-induced nano-crystallization means that mechanical deformation can drive crystalline solids far from their equilibrium state by introducing structural or chemical defects and recrystallization[27].

The structure refinement is related to phase transformation during annealing. The volume ratio of α"-$Fe_{16}N_2$ is increased consequently. In strain-induced phase transformation, plastic deformation of the parent phase creates a proper defect structure which acts as an embryo for the transformation product. Specifically, in austenitic FeN material embryos are formed at the intersections of the microscopic stacking faults, planar defect and nanosize grains. The mechanism for such kind of deformation-induced crystallization, as shown in FIG. 9(d), can be explained as follows. The formation of this boundary is probably due to the uneven thickness of the samples. Some thin regions under high stress preferentially nucleate cracks during the tensile annealing. Along these cracks, a number of smaller cracks are formed, oriented approximately parallel to the fracture surface. Finally, the tensile fracture causes such nanocrystal formation.

The appearance of planar defects and smaller grains correlates with the increment of the coercivity. We suspect that the coercivity of the wire samples is controlled in general by a domain wall pinning mechanism at a precipitate structure throughout the grains.

For the sample with 0.4% strain, shown in FIG. 9(d), a further magnified STEM image is shown in FIG.10. By using electron diffraction on different regions inside and outside of the generated nanocrystal entity it can be seen that there is a clear difference in terms of ordering, as shown in FIG. 10(a). FIG.10(b) shows the corresponding crystalline phases in electron diffraction pattern.

Combined with XRD patterns in FIG.3, the prepared sample can be considered as partially ordered $Fe_{16}N_2$+Fe_8N martensite phase. In this case, a degree of N site ordering (D) can be defined by comparing the intensity ratio of $I(002)/I(004)^2$, where I(002) and I(004) denote the intensity of peaks according to the electron diffraction pattern, as shown in FIG.10(a). The processed images clearly show areas of diffraction patterns with varying degrees of ordering. The ordering parameter inside the grain is measured to be 0.85 while that outside the grain to be 0.21. Generally, the area inside the grain has higher order than the area outside the grain. Some of the original order in the grain analyzed may have been degraded by electron beam damage. The difference in ordering may be caused by the variation of strain concentration on the sample.

The sample prepared by the strained wire method appears to be an anisotropic magnet since the uniaixial strain leads to an easy-axis alignment[28]. FIG. 11 shows the hysteresis loops of the sample produced under 0.4% strain. Loop 'a' corresponds to perpendicular to long axis of wire, while loop 'b' is along long axis result. An obvious anisotropic magnetic property can be observed. The Mr/Ms ratio at the in-plane is 0.62.

The physical mechanism of the strained-wire method is obviously related to the transformation induced by plastic deformation, since in this case, the moving defects created during this deformation are thought to take a very important role in the phase transformation process. In this particular, we have shown that the martensitic products can be drastically different from other α"-$Fe_{16}N_2$ samples reported by previous researchers, showing obvious hard magnetic property and higher magnetization saturation value at the same time. In our case, it is suggested that the martensitic material with suitable tuned microstructures is a good candidate for rare-earth-free permanent magnet.

For the prepared sample with energy product up to 9 MGOe, it is worth noting that its hysteresis loop is in nearly square shape. This is different from wasp-taille shape of hysteresis loop observed in sample with soft and hard phase co-existed[29]. The hysteresis shape and coercivity are varied with different ratio between soft and hard phase[30]. For the 9 MGOe sample with nearly square hysteresis loop, we believe this is resulted by the interplay among exchange spring effect, alignment of $Fe_{16}N_2$ phase and the generated defects as pinning sites.

The exchange spring effect is caused by the interaction between soft and hard phase. The volume ratio of α"-$Fe_{16}N_2$ in the 9 MGOe sample is estimated to be 37% by using XPS method[26]. Based on the TEM result on its microstructure, as shown in FIG.9(d), the generated grain size is about 25 nm, while the ordering parameters inside and outside grain are different. This observation means that the phase distribution in the sample isn't homogeneous, which results some deviation from the theoretical wasp-taille shape.

The alignment of $Fe_{16}N_2$ phase by the applied stress during post-annealing is another reason for the deviation on the shape of hysteresis loop. The uniaxial stress influences the preference of orientation during phase transformation from austenite to martensite. The prepared sample does not follow the model of random-anisotropy nanostructure anymore. Further characterizations on the sample's structure and orientation need to be investigated on the sample, which would be helpful to set up a suitable micro-magnetic model for this novel magnetic material.

The generated defects, as shown in FIG.10(a), act as pinning site in the sample. The appearance of planar defects and smaller grains correlates with the increment of the coercivity and the shape of hysteresis loop.

Above all, the square shape of hysteresis loop in the prepared FeN sample is a synthesis effect of several aspects, including its unique microstructure, the alignment on (001) orientation by the external strain, and also the generated defects. More detail investigation would be needed to clarify the mechanism.

The generated defects, as shown in FIG.10(a), act as pinning site in the sample. The appearance of planar defects and smaller grains correlates with the increment of the coercivity and the shape of hysteresis loop.

The grain recrystallization induced transformation is to be thought of as a defect accumulation of the material, concurrent with the deformation mode of the mother phase. The phenomenon of defect accumulation is demonstrated by STEM characterization on the strained samples, as shown in FIG. 10.

For the deformation of the mother phase, different variation of degree ordering inside and outside of the generated grain, as shown in FIG.10, reveals a spontaneous transformation of mother phase with defect accumulation.

The defect accumulation is also considered as the propagation of the plastic deformation. The defect rich area is the intersection of the active planes, accounting for the lath martensite, where conditions are extremely favorable for transformation dislocations to come together with high stress concentrations. The required strain for the martensitic deformation is controlled both by the rate of variation of Gibbs free energy and by the efficiency of recrystallization grains involved. Our current knowledge of Gibbs free energy and entropy of transformation in an α''-$Fe_{16}N_2$ system is very limited and further investigation of this system will be required to account for the association of defect generation with preferential ordering of mother phase.

V. CONCLUSIONS

We have here proposed and demonstrated a novel synthesis method for bulk anisotropic $Fe_{16}N_2$ materials, named the "strained wire method." Based on this method, an anisotropic iron nitride magnet with 9 MGOe was achieved. We demonstrated that the applied uniaxial strain could largely influence the phase transformation, the microstructure and magnetic properties of α''-$Fe_{16}N_2$wire samples. The external induced energy by strain can compensate for the shortage of thermal annealing energy during phase transformation and can be used to protect the martensitic phase formation. This is a potential synthesis method for bulk anisotropic FeN magnets compatible with the industrial manufacturing process.

ACKNOWLEDGMENT

This work was supported in part by ARPA-E (Advanced Research Projects Agency-Energy) BCT $Fe_{16}N_2$ Magnet project under contract No.0472-1595. Parts of this work were carried out in the Characterization Facility, which receives partial support from the NSF through the NSF Minnesota MRSEC program under Award Number DMR-0819885.Dr. Jian-Ping Wang has equity and royalty interests in, and serves on the Board of Directors and the Scientific Advisory Board, of Niron Magnetics LLC, a company involved in the commercialization of FeN magnets. The University of Minnesota also has equity and royalty interests in Niron Magnetics LLC. These interests have been reviewed and managed by the University of Minnesota in accordance with its Conflict of Interest policies.

References

1 S. Chu and A. Majumdar. Opportunities and challenges for a sustainable energy future. *Nature***488**, 294-303 (2012).

2 J. P. Wang, N. Ji, X. Liu, Y. Xu, C.Sanchez-Hanke, Y. Wu, F.M.F.de Groot, L. F.Allard and E. Lara-Curzio. Fabracation of $Fe_{16}N_2$ Films by Sputtering Process and Experimental Investigation of Origin of Giant Saturation Magnetization in $Fe_{16}N_2$. *IEEE Transactions on Magnetics***48**, 1710-1717 (2012).

3 Jack, K. H.The occurrence and the crystal structure of α''-iron nitride; a new type of interstitial alloy formed during the tempering of nitrogen-martensite. *Proc. R. Soc. London. A***208**, 216-224 (1951).

4 T.K.Kim, M. T. New Magnetic Material Having Ultrahigh Magnetic Moment. *Appl.Phys.Lett.* **20**, 492-494 (1972).

5 D.C.Sun, E. Y. J., M.B.Tian, C.Lin and X.X.Zhang. Epitaxial single crystal $Fe_{16}N_2$ films grown by facing targets sputtering. *J.Appl.Phys.***79**, 5440-5442 (1996).

6 H.Shinno, K. S. Effects of film thickness on formation processes of $Fe_{16}N_2$ in nitrogen ion-implanted Fe films. *Surface and Coatings Technology***103-104**, 129-134 (1998).

7 H.Takahashi, H. S., M.Takahishi. Structure and magnetic moment of $Fe_{16}N_2$ sputtered film. *J.Magn.Magn.Mater.***174**, 57-69 (1997).

8 J.M.D.Coey. The magnetization of bulk α˝-$Fe_{16}N_2$ (invited). *J.Appl.Phys,***76**, 6632-6636 (1994).

9 Kensuke Nakajima, S. O. Nitrogen-implantation-induced transformation of iron to crystalline Fe16N2 in epitaxialiron films. *Appl.Phys. Lett.***54**, 2536-2538 (1989).

10 M.A.Brewer, C. J. E., K.M.Krishnan, T.Kobayashi, A.Nakanishi. Magnetic and physical microstructure of $Fe_{16}N_2$ films grown epitaxially on Si(001). *J.Appl.Phys.***81**, 4128-4130 (1997).

11 M.Q.Huang, W. E. W., S.Simizu, S.G.Sankar. Magnetism of α΄-FeN alloys and α˝-($Fe_{16}N_2$)Fe nitrides. *J. Magn. Magn. Mater***135**, 226-330 (1994).

12 S.Okamoto, O. K., Y.Shimada. α˝-$Fe_{16}N_2$ phase epitaxially grown by sputter beam method. *Journal of Appl.Phys.***79**, 5250-5252 (1996).

13 T.Weber, L. d. W., F.W.Saris, P.Schaaf. Search for giant magnetic moments in ion-beam-synthesized α˝-$Fe_{16}N_2$. *Thin Solid Films***279**, 216-220 (1996).

14 Xiaohua Bao, R. M. M., Massimo Carbucicchio. Synthesis and properties of α˝-$Fe_{16}N_2$ in magnetic particles. *Journal of Applied Physics***75**, 5870-5872 (1994).

15 Y. Sugita, H. T., M. Komuro, K. Mitsuoka, and A. Sakuma. Magnetic and Mössbauer studies of single-crystal $Fe_{16}N_2$ and Fe-N martensite films epitaxially grown by molecular beam epitaxy(invited). *J. Appl. Phys***76**, 6637-6641 (1994).

16 Y.Sugita, H. T., M.Komuro, M.Igarashi, R.Imura, T.Kambe. Magnetic and electrical properties of singlephase, singlecrystal $Fe_{16}N_2$ films epitaxially grown by molecular beam epitaxy(invited). *J.Appl.Phys***79**, 5576-5581 (1996).

17 Takashi Ogi, A. B. D. N., Yutaka Kisakibaru, Toru Iwaki, Keitaro Nakamura, Kikuo Okuyama. Facile synthesis of single-phase spherical a"-$Fe_{16}N_2$/Al_2O_3 core-shell nanoparticles via a gas-phase method. *J. Appl. Phys***113**, 164301 (2013).

18 Y. Jiang, J. Liu, P. K.Suri, G. Kennedy, N. N. Thadhani, D. J. Flannigan, J. P. Wang. Preparation of an a"-$Fe_{16}N_2$ magnet via a ball milling and shock compaction approach. *Advanced Engineering Materials*, doi: 10.1002/adem.201500455 (2015).

19 Y.Jiang, M.Mehedi, E.Fu, Y.Wang, L.F.Allard, J.P.Wang, Synthesis of Fe16N2 compound free-standing foils with 20 MGOe magnetic energy product by nitrogen ion-implantation. Scientific Reports 6, 25436 (2016).

20 T. Ogawa, Y. O., Ruwan Gallage, Naoya Kobayashi, Naoaki Hayashi, Yoshihiro Kusano. Challenge to the synthesis of a"-$Fe_{16}N_2$ compound nanoparticle with high saturation magnetization for rare earth free new permanent magnetic material. *Applied Physics Express***6**, 073007 (2013).

21 K. Takagi, M. A., Kimihiro Ozaki, Naoya Kobayashi, Tomoyuki Ogawa, Yasunobu Ogata, Migaku Takahashi. High-pressure sintering behavior of a"-$Fe_{16}N_2$ nanopowder. *J. Appl. Phys***115**, 103905 (2014).

22 C.E.Krill III, L. H., D.Michels, H.Natter, A. Fitch, O.Masson, R.Birringer. Size-dependent grain-growth kinetics observed in nanocrystalline Fe. *Physical Review Letters***86**, 842-845 (2001).

23 See Supplemental Material at [URL will be inserted by publisher] for evaluation of annealing temperature for α"-$Fe_{16}N_2$ material, whole process description, structure of designed fixture, mechanical properties of prepared α"-$Fe_{16}N_2$ material.

24 Y. Jiang, V. Dabade, M. P. Brady, O. Rios, R. D. James, and J. P. Wang. 9T high magnetic field annealing effects on FeN bulk sample. Journal of Applied Physics **115**, 17A758(2014).

25 E.H.Du Marchie Van Voorthuysen, N. C. C., D.O.Boerma. Low-Temperature Extension of the Lehrer Diagram and the Iron-Nitrogen Phase Diagram. *Matellurgical and Materials Transactions A***33A**, 2593-2598 (2002).

26 Y. Jiang, X. Z., M. Al Mehedi, M. Yang, J. P. Wang. A method to evaluate a"-$Fe_{16}N_2$ volume ratio in FeN bulk material by XPS. *Materials Research Express***2**, 116103 (2015).

27 W.H.Jiang, M. A. Mechanically-assisted nanocrystallization and defects in amorphous alloys: A high resolution transmission electron microscopy study. *Scripta Materialia***54**, 333-336 (2006).

28 L. Zhang, L.-Q. C., Qiang Du. Morphology of Critical Nuclei in solid-State Phase Transformations. *Physical Review Letters***98**, 265703 (2007).

29 R.Skomski. Nanomagnetics. *J.Phys.:Condens. Matter* **15**, R841-R896 (2003).

30 Joseph J. Becker. Rapidly quenched metals for permanent magnet materials. *Journal of Applied Physics* **55**, 2067-2072 (1984).

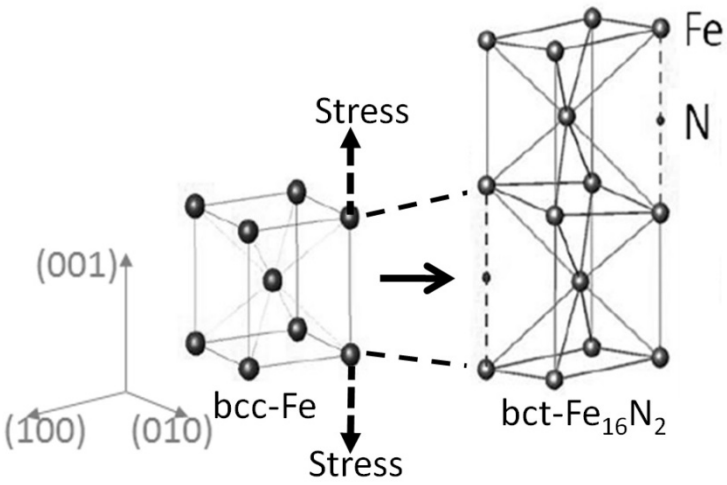

FIG.1 Schematic of effect of stress on phase transformation from bcc to bct structure. The stress, either external force or magnetic field, is applied along c-axis to assist for the phase transition.

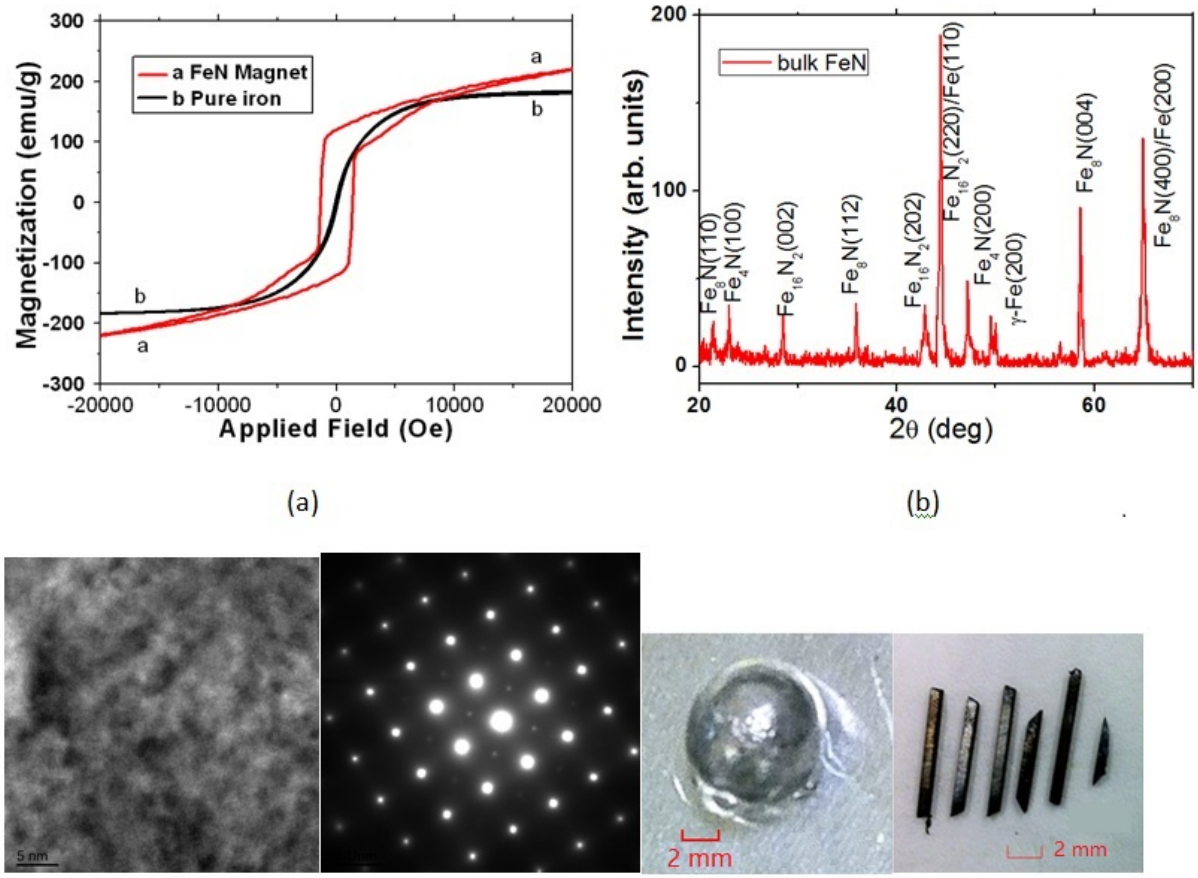

FIG.2 Characterization results of the prepared FeN permanent magnet and sample pictures

(a) Hysteresis loop of an FeN magnet(Loop 'a'), showing a near square loop, with a coercivity of 1220 Oe. The magnetization at the 2T field is 220 emu/g. The saturation magnetization is 245emu/g at the 4.5T field. The energy product at room temperature is calculated to be 9MGOe. The hysteresis loop of pure iron is shown in loop 'b' as a comparison.

(b) X-ray diffraction (XRD) pattern of the FeN magnet, showing that the prepared sample is a mixture of $Fe_{16}N_2$, Fe_8N, Fe_4N and Fe phases.

(c) TEM image and diffraction pattern of the FeN bulk sample, showing a super-lattice diffraction pattern.

(d) Actual pictures of the samples. In the strained wire method, the sample is cut into wire shape, which is convenient for application oftensile force along the uniaxial direction.

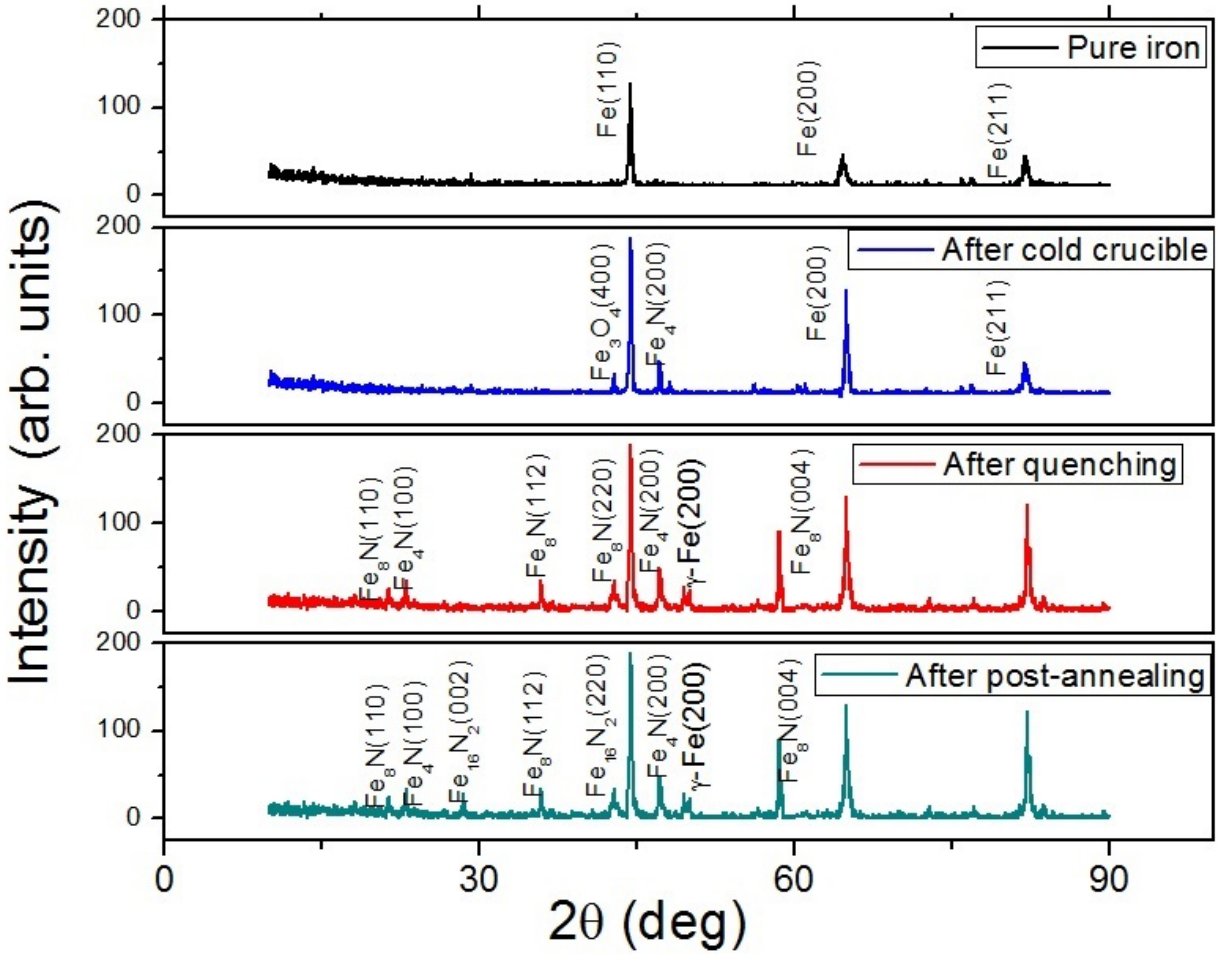

FIG.3 XRD patterns for samples (a) Pure iron; (b) After cold crucible melting, showing crystalline intensities of iron is enhanced after cold crucible ; (c) After quenching, part of iron is transferred into α′-Fe_8N phase and γ′-Fe_4N phase. There is also γ-Fe; (d) After post-annealing, part of α′-Fe_8N is transformed into α″-$Fe_{16}N_2$.

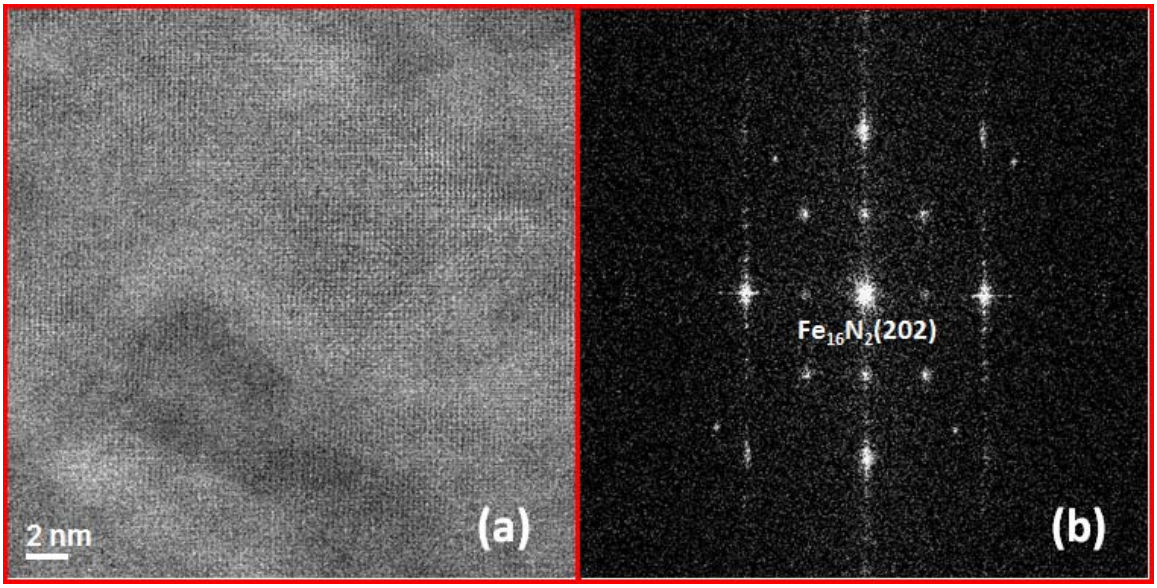

FIG.4 Microstructure and diffraction patterns of the sample (a) High-resolution STEM bright-field image. (b) Corresponding diffractogram of sample, showing the α"-$Fe_{16}N_2$ phase.

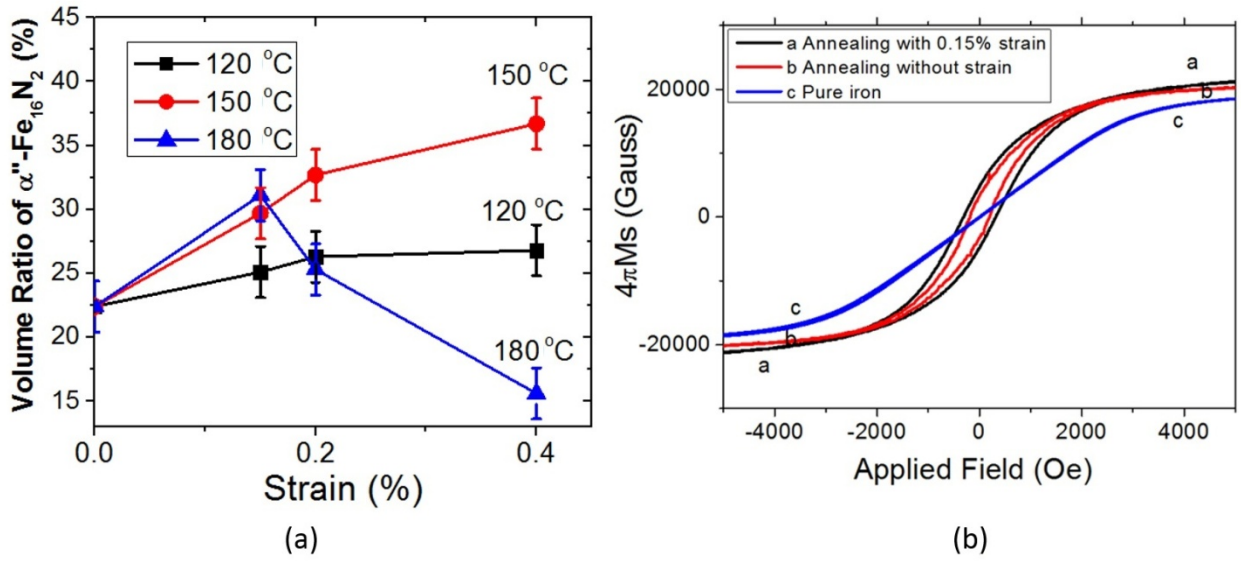

FIG.5 (a) Volume ratio of α”-$Fe_{16}N_2$ phase by uniaxial tension as a function of strain at different temperatures. At 150 °C, the volume ratio keeps increasing at different strains, showing positive effect of strain on the martensite phase transformation. (b)Hysteresis loops on samples with 150 °C annealing temperature; loop ‘a’ with 0.15 % strain, loop ‘b’ without strain and loop ‘c’ pure iron as baseline.

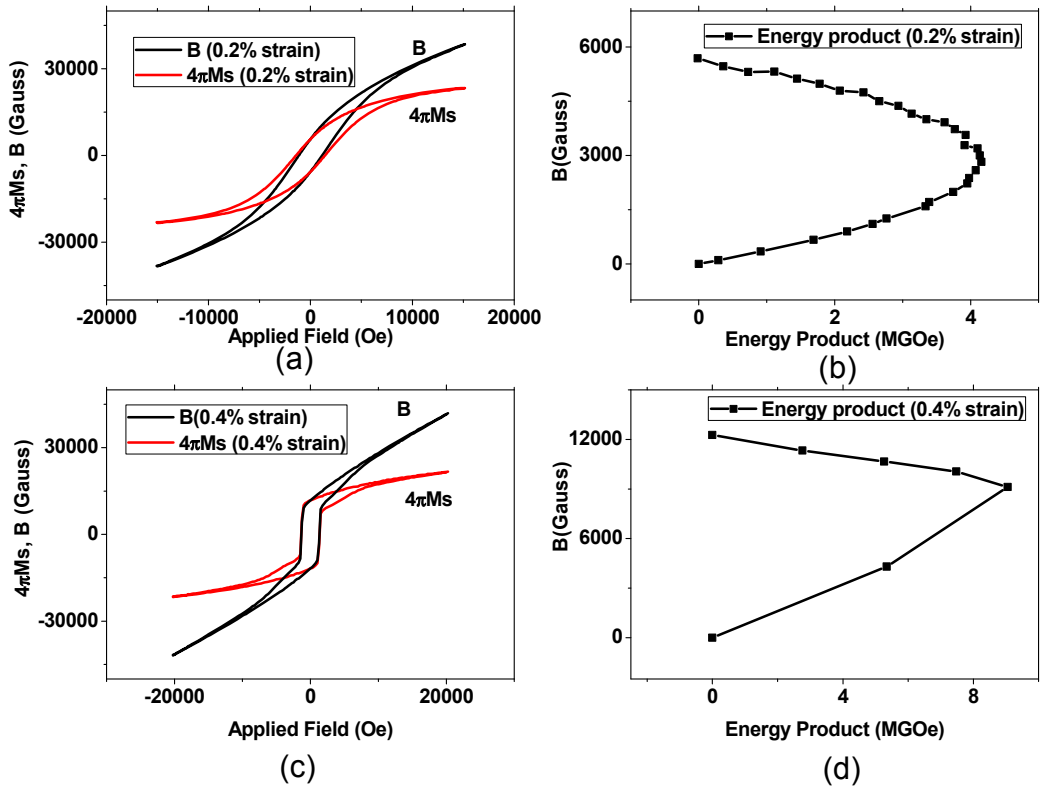

FIG.6 Magnetic properties of samples with different forces (a) Hysteresis loop of sample annealed with 0.2% strain; (b) Energy product of sample annealed with 0.2% strain; (c) Hysteresis loop of sample annealed with 0.4% strain; (d) Energy product of sample annealed with 0.4% strain.

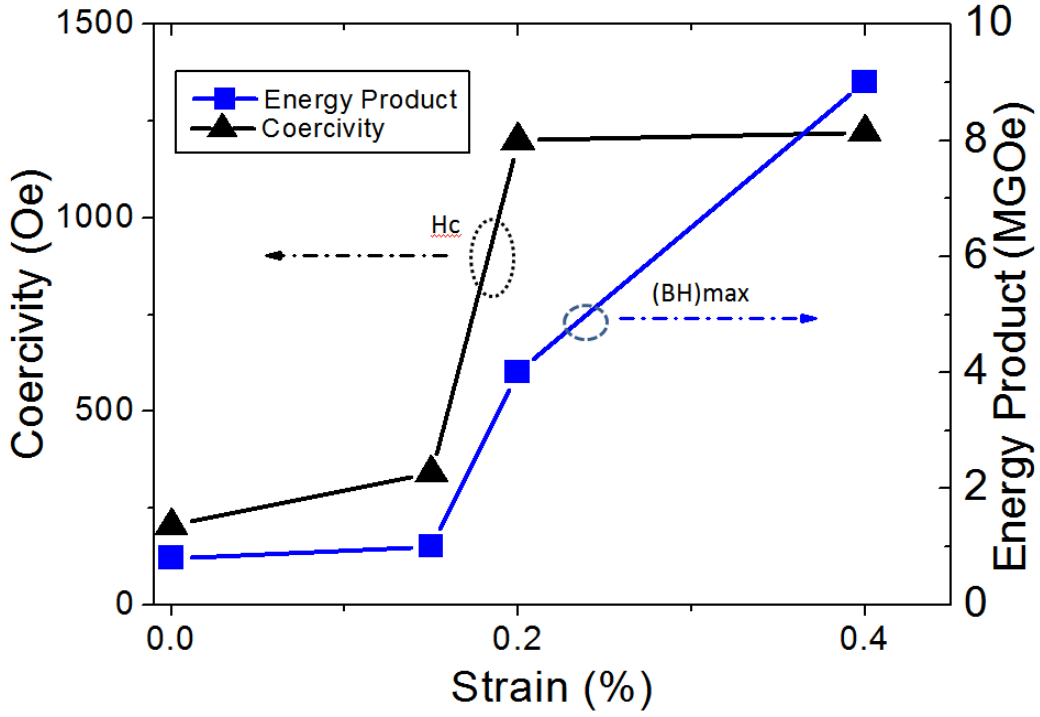

FIG.7 Influence of applied uniaxial strain on samples' coercivity and energy product, showing a 0.4% strain can lead to energy product up to 9 MGOe and coercivity up to 1220 Oe.

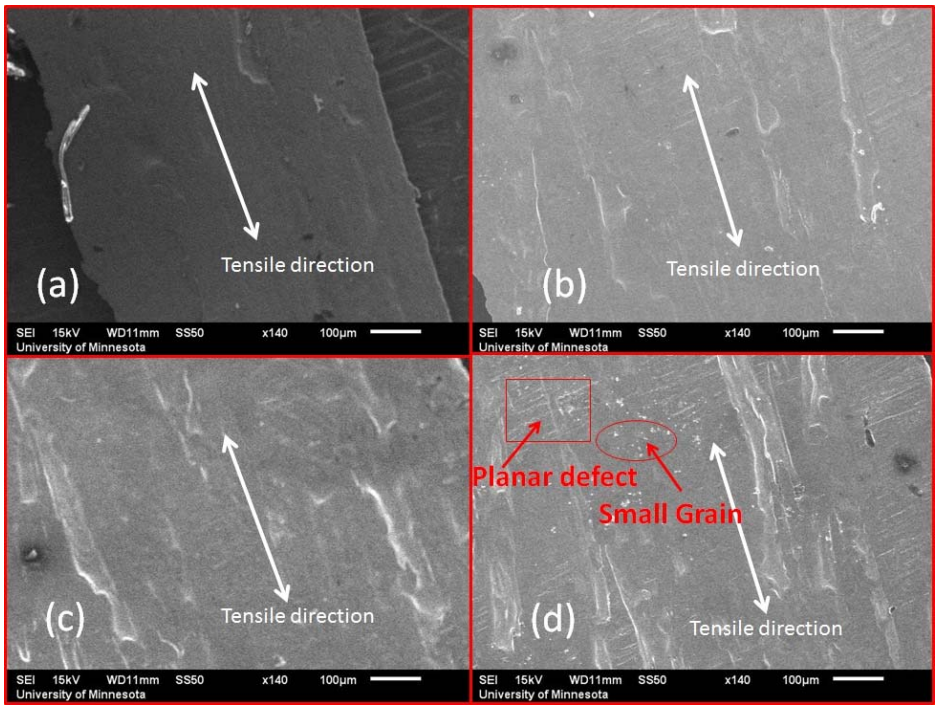

FIG.8 Scanning electron microscope (SEM) characterizations on samples with different strains at 150 °C annealing temperature for 40hrs (a) Without strain; (b) With 0.15% strain along tensile direction as shown; (c) With 0.2% strain, showing more microstructure; (d) With 0.4% strain, showing microstructures, planar defects and smaller grains on sample.

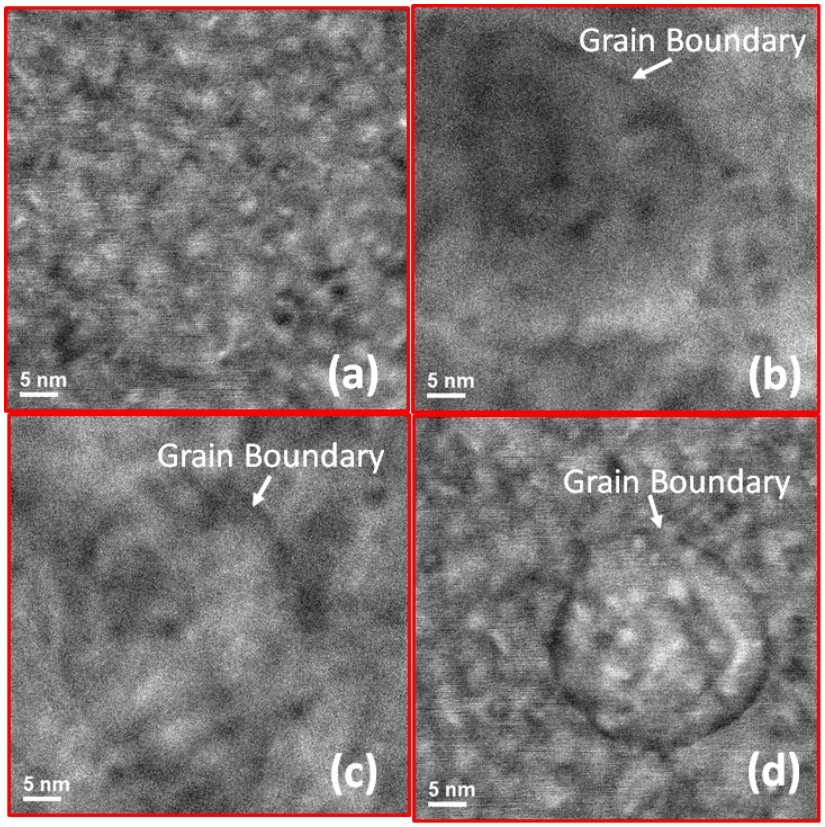

FIG.9 The high-resolution STEM characterizations on samples with different strains at 150 °C annealing temperature for 40hrs (a) Without strain; (b) With 0.15% strain, grain boundary appearsas shown; (c) With 0.2% strain, showing more obvious boundary; (d) With 0.4% strain, showing clear grain boundary on sample and a whole grain is formed.

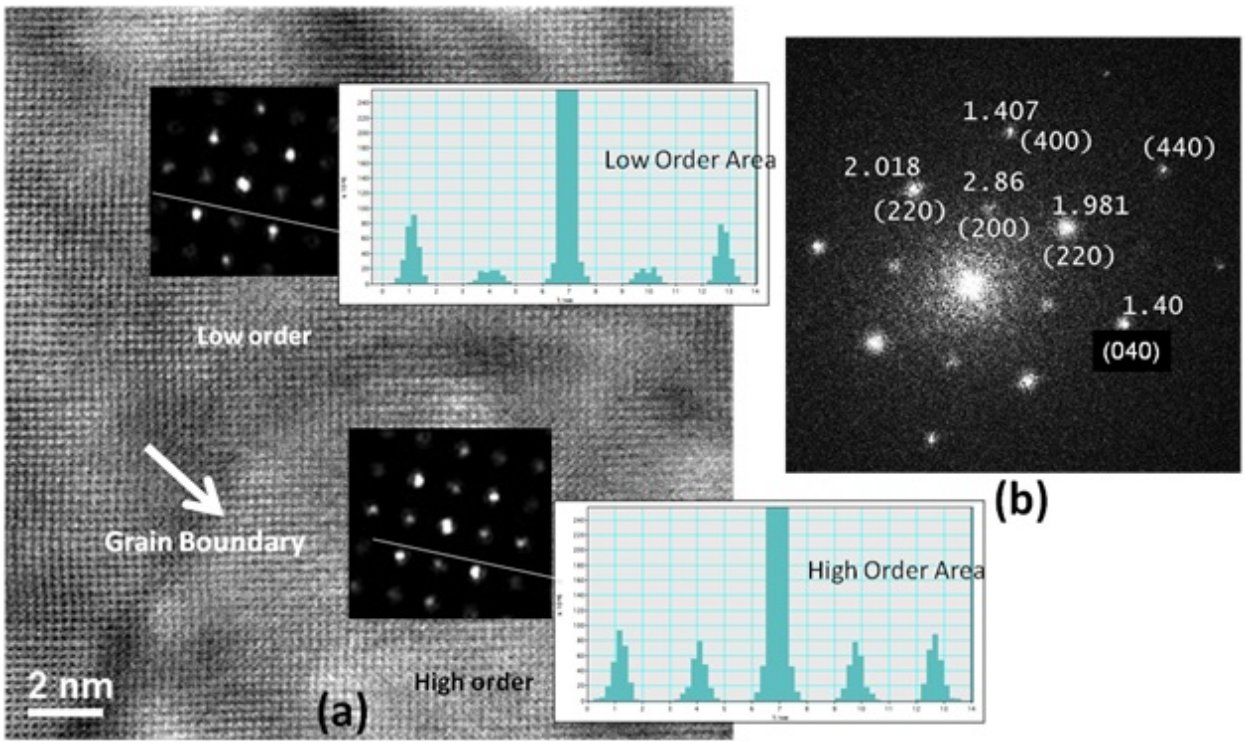

FIG.10 (a)The high-resolution STEM characterization of a sample produced at 150 °C annealing temperature for 40 hrs with 0.4% strain. Insets show the electron diffractions on different regions inside and outside of the generated nanocrystal entity. (b) The corresponding crystalline phases in electron diffraction, as annotated with orientation and space. The area inside the grain has higher order than the area outside the grain. The difference in ordering may be caused by the variation of strain concentration on the sample.

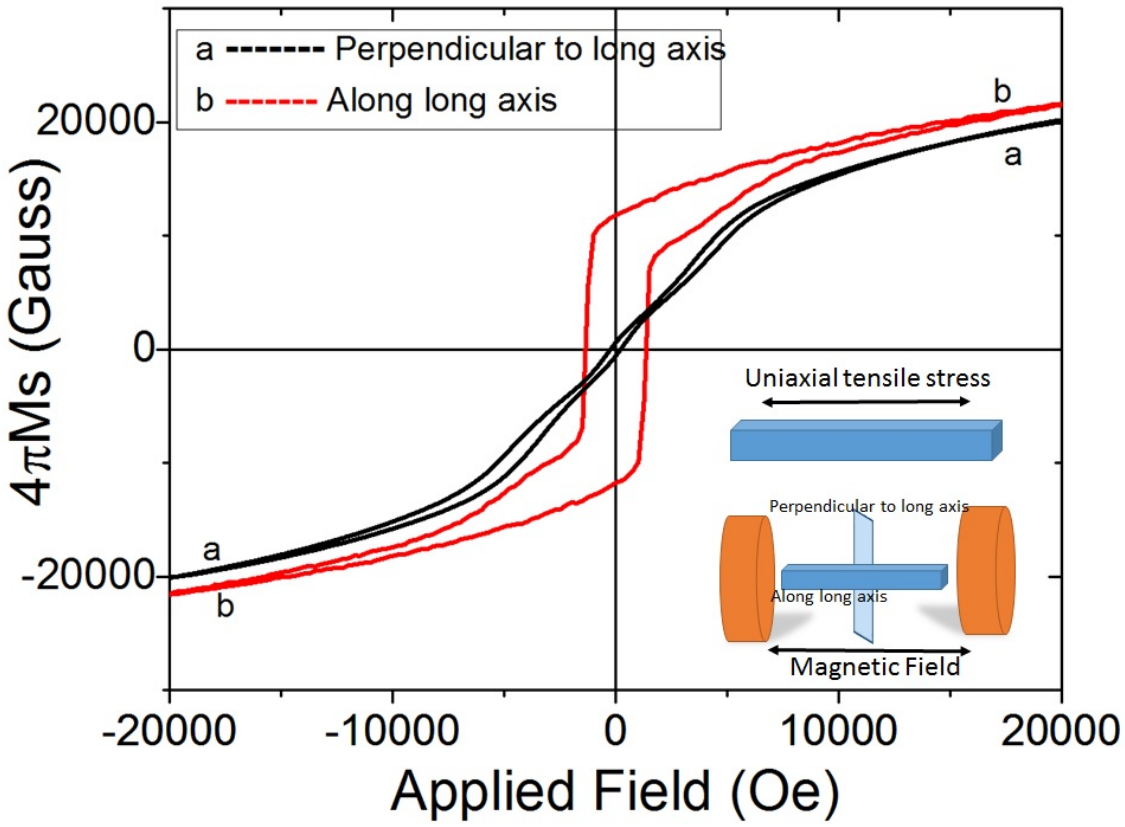

FIG. 11 Hysteresis loops of the sample with 0.4% strain. Loop 'a'isperpendicular to the long axis of the wire, while loop 'b' is along the long axis of wire. An obvious anisotropic magnetic property can be observed. The Mr/Ms ratio at in-plane is 0.62.